

Selected Paper

CdS Nanoparticles Exhibiting Quantum Size Effect by Dispersion on TiO_2: Photocatalytic H_2 Evolution and Photoelectrochemical Measurements

Kiyonori Ogisu,[1] Kazuhiro Takanabe,[1] Daling Lu,[2] Masaki Saruyama,[3] Takahiro Ikeda,[3] Masayuki Kanehara,[3] Toshiharu Teranishi,[3] and Kazunari Domen*[1]

[1]Department of Chemical System Engineering, The University of Tokyo, 7-3-1 Hongo, Bunkyo-ku, Tokyo 113-8656

[2]Chemical Resources Laboratory, Tokyo Institute of Technology, 4259 Nagatsuta, Midori-ku, Yokohama 226-8503

[3]Graduate School of Pure and Applied Sciences, University of Tsukuba, Tennodai, Tsukuba 305-8571

Received November 20, 2008; E-mail: domen@chemsys.t.u-tokyo.ac.jp

Uniformly sized CdS nanoparticles exhibiting quantum size effect have been synthesized as a suspension in hexane solution containing oleic acid and 9-octadecenylamine as protective ligands. Our study focuses on utilizing the intrinsic optical property of the nanoparticles for photocatalytic H_2 evolution and photoelectrochemical reaction by immobilizing oxide substrate and removing protective ligands. Immobilized CdS nanoparticles on TiO_2 were found to maintain their original particle size and optical property after impregnation and removal of the protective ligands by oxidative heat treatment and/or alkali treatment. The photocatalytic H_2 evolution rates in Na_2S–Na_2SO_3 solution under visible light were strongly affected by the CdS particle size (quantum size effect), CdS loading amount, and TiO_2 surface area. High photoanodic current was observed for CdS/TiO_2 sprayed on a fluoride-doped tin oxide (FTO) electrode, functioning as an n-type semiconductor. The knowledge acquired in this study can be extended for further development in the field of nanoparticle materials covered with protective ligands.

Hydrogen production from water using a semiconductor photocatalyst is a key technology for achieving sustainable energy conversion. Some oxides, such as TiO_2,[1] $SrTiO_3$,[2] and $NaTaO_3$,[3] function as highly efficient photoelectrodes and photocatalysts under UV irradiation. To utilize sunlight however, a candidate material must possess appropriate visible light absorption properties. Several chalcogenide materials, such as CdS,[4] $NaInS_2$,[5] and $(AgIn)_xZn_{2(1-x)}S_2$,[6] are promising photocatalysts because they exhibit appropriate absorption of visible light.

Among these chalcogenide materials, CdS has received particular attention as a photocatalyst in recent years. It has potential as an efficient photocatalyst for water splitting because of its visible-light absorption (B.G. = 2.4 eV) and the position of its band edges. The material itself however, is unable to split H_2O to form H_2 and O_2, and the material decomposes in standard aqueous solution during photoreaction.[7–9] To enable the use of this material, many researchers have demonstrated the hydrogen evolution reaction in reducing agents such as EDTA, S^{2-}, SO_3^{2-}, or phosphinate ions to prevent photoanodic dissolution.[7–13] Stabilization of CdS on support materials such as TiO_2, AgI, ZnO, or HgS has also been investigated,[14–16] and may improve the efficiency of charge separation and photoreaction efficiency.

Semiconductor particles with diameters on the order of nanometers exhibit unique size-dependent properties, such as the quantum size effect which drastically alters electrical properties.[17–20] In the conventional infinite-depth well model,[21] the excitation energy level E_{ln} of an ultra-small semiconductor particle with radius R is a function of the band gap energy E_g of bulk semiconductor and kinetic energy (eq 1). The kinetic energy can be calculated as the energy of a particle in a box having a spherically symmetric square well potential of infinite depth:

$$E_{ln} = E_g + \left(\frac{\hbar^2}{2m^* R^2}\right)\phi_{ln}{}^2 \quad (1)$$

where m^* is the reduced effective mass of the conduction band electron and valence band hole. ϕ_{ln} is the n-th root of the spherical Bessel function of l-th order.[21] The equation indicates that the band gap of nanosize CdS ($\leq$6 nm) is larger than that of CdS bulk, and the gap increases with decreasing particle size. Thus, nanoparticles show distinct oxidative and reductive abilities for photocatalytic reactions. Decreasing particle size also leads to an increase in surface area, altering mechanical, thermal, and catalytic properties.

We synthesized well-tuned CdS nanoparticles with a very narrow size-distribution in the presence of protective ligands suspended in organic solution.[22–24] Several studies have assessed the use of quantum dot CdS sensitized TiO_2 as photocatalyst material. In contrast to many other studies, where CdS was synthesized from Cd solution and immobilized on a support material simultaneously by in situ electrochemical methods or photodeposition,[25–32] we immobilized already-prepared CdS nanoparticles on TiO_2 to maintain the original particle sizes and avoid aggregation upon removal of the protective ligands and during photoreactions. The immobilization of uniformly sized CdS nanoparticles in a controlled

Published on the web April 11, 2009; doi:10.1246/bcsj.82.528

manner also enables us to elucidate details of particle size effects, e.g., quantum size effects. By varying the immobilization method, CdS particle size, surface area of the support, and the amount of CdS and Pt (as a co-catalyst), the immobilized CdS/TiO_2 catalysts were tested for photocatalytic H_2 evolution and photoelectrochemical reactions in the presence of Na_2S/Na_2SO_3 sacrificial reagent under visible light irradiation. This study clearly shows the beneficial effects of immobilizing nanoparticles with quantum size effects, providing high efficiency and stability for photocatalytic reactions.

Experimental

Immobilization of CdS Nanoparticles on TiO_2 Support. CdS nanoparticles were synthesized based on a previously reported method.[22–24] The CdS nanoparticles were immobilized on TiO_2 photocatalysts then prepared by heat treatment and alkali treatment. CdS nanoparticles (1.6 ± 0.2, 2.9 ± 0.3, 3.4 ± 0.4, 4.1 ± 0.6, and 12.5 ± 1.6 nm) suspended in hexane solution (Kanto Chemical, 96%) with oleic acid (bp 468 K) and oleyl amine (bp 441 K) as protective ligands were added to TiO_2 (Degussa, P25) and mixed by ultrasonic agitation until the hexane was vaporized at 298 K. In the heat treatment, dried samples were heated at 473 or 623 K for 5 h in air. In the alkali treatment method, dried samples were added to 50 mL of 0.1 M ($1\ M = 1\ mol\ dm^{-3}$) NaOH solution and stirred for 1 h to remove protective ligands. The samples were filtered and washed with 50 mL of distilled water, then dried at 343 K in static air.

Characterization. Differential thermal analysis and thermogravimetry (TG-DTA; TG 8120, Rigaku) were used to study the crystallization, decomposition, melting, and sublimation processes. The crystalline structure of the catalyst was examined by powder X-ray diffraction (XRD; Panalytical X'Pert Pro MPD). The optical properties were analyzed with an ultraviolet–visible diffuse reflectance spectrometer (DRS; V-560, Jasco). Particle size and photocatalyst morphology were examined by transmission electron microscopy (TEM; JEM-2010F, JEOL). The elemental compositions were probed by X-ray fluorescence (XRF; Element Analyzer JSX-3202C, JEOL) and energy-dispersive X-ray spectroscopy (EDX; Emax-7000, Horiba). The Brunauer–Emmett–Teller (BET) specific surface area was measured using a Coulter SA-3100 instrument at 77 K.

CdS/TiO_2 electrodes were fabricated by spreading a viscous slurry of the prepared powder on fluorine-doped tin oxide (FTO) transparent conductive glass (ca. 20 Ω; Asahi Glass). Before spreading the slurry, the substrates were ultrasonicated, first in acetone and then in distilled water. The slurry consisted of the sample (0.1 g), water (100 mL), acetylacetone (100 mL), and 10 mL of surfactant (Triton X-100, Aldrich). The electrode (coated area: $1 \times 4\ cm^2$) was then heated in air at 573 K for 1 h to remove organic solvent and surfactant and to improve the contact between catalyst and substrate.

Current–voltage and current–time curves were measured using a conventional Pyrex electrochemical cell attached to a planar side window. The cell consisted of a prepared electrode, a platinum wire counter electrode (diameter: 1 mm, length: 250 mm), and an Ag/AgCl reference electrode. Aqueous solutions of 0.1 M Na_2S–Na_2SO_3 were used as electrolytes. The electrolytes were saturated with argon prior to each electrochemical measurement, and electrode potential was controlled by a potentiostat (HZ-5000, Hokuto Denko or SDPS-501C, Syrinx). Light irradiation was performed using a 300 W xenon lamp with a cutoff filter ($\lambda \geq 420$ nm).

Photocatalytic Reactions. H_2 evolution reactions from 0.1 g of CdS/TiO_2 catalysts were performed using an aqueous solution (200 cm^3) in the presence of 0.1 M Na_2S and 0.1 M Na_2SO_3 as sacrificial electron donors. A Pt co-catalyst was loaded by photodeposition in the presence of the sacrificial electron donors (0.1 M Na_2S and 0.1 M Na_2SO_3) using $H_2PtCl_6 \cdot 6H_2O$ (Aldrich; ≥37.50% as Pt).

Photocatalytic reactions were carried out in a Pyrex reaction vessel connected to a closed gas circulation system. The reaction solution was evacuated several times to remove residual air from the reaction solution, and then irradiated under visible light using a 300 W xenon lamp via a cutoff filter ($\lambda \geq 420$ nm) to eliminate ultraviolet (UV) light and a water filter to block infrared light. The amounts of H_2 evolved were measured by gas chromatography (GC-8A, Shimadzu; MS-5A column, TCD, Ar carrier). The catalyst is denoted as Pt(n)/M wt% CdS(D)/TiO_2, where n, M, and D are the wt% of Pt based on CdS, wt% of CdS based on TiO_2, and particle size in nm. P25 was used as a TiO_2 support unless otherwise noted.

Results and Discussion

Characterization of CdS Nanoparticles. The different sized CdS nanoparticles (1.6–12.5 nm) protected by (*Z*)-9-octadecenylamine and oleic acid were prepared according to literature methods.[22–24] Figure 1 shows the TEM images of these CdS nanoparticles. All CdS nanoparticles were monodisperse and soluble in nonpolar solvents, such as hexane, toluene, and chloroform. As shown in Figure 2, UV–vis spectra

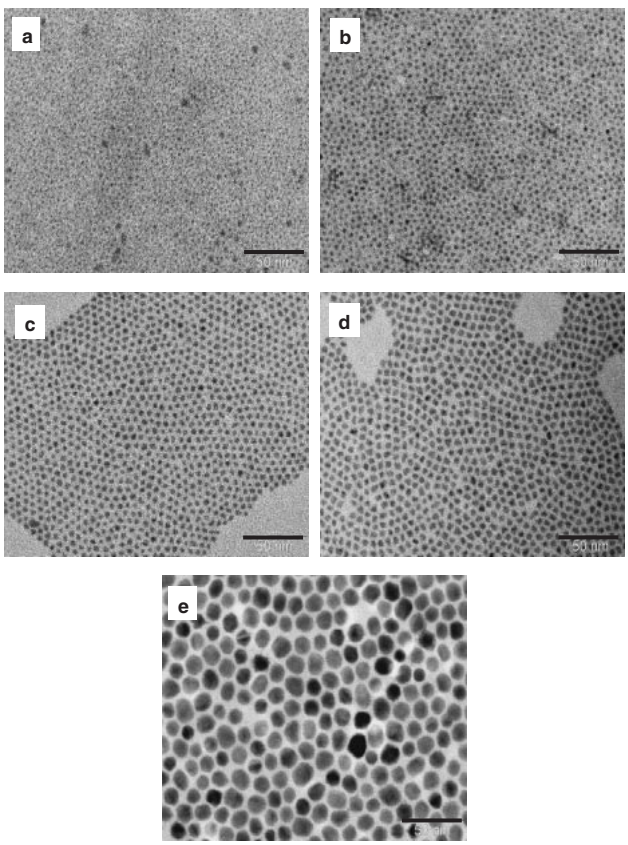

Figure 1. TEM images of CdS nanoparticles with (a) 1.6 ± 0.2, (b) 2.9 ± 0.3, (c) 3.4 ± 0.4, (d) 4.1 ± 0.6, and (e) 12.5 ± 1.6 nm in size. The scale bars indicate 50 nm.

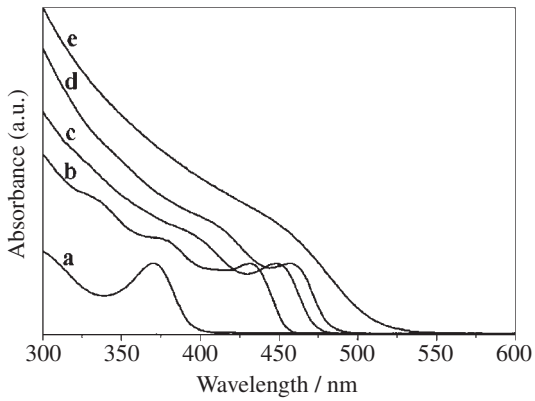

Figure 2. UV–vis spectra of *n*-hexane solution of CdS nanoparticles with (a) 1.6 ± 0.2, (b) 2.9 ± 0.3, (c) 3.4 ± 0.4, (d) 4.1 ± 0.6, and (e) 12.5 ± 1.6 nm in size.

of 1.6, 2.9, 3.4, and 4.1 nm sized CdS nanoparticles showed exiton peaks at 370, 432, 449, and 457 nm, respectively, due to the quantum size effect, whereas 12.5 nm CdS nanoparticles showed bulk like spectrum.

Immobilization of CdS Nanoparticles on TiO_2 Support. Immobilization of CdS nanoparticles on TiO_2 support was accomplished by sonicating TiO_2 suspension in CdS hexane solution at room temperature. Hexane proved to be the most effective solvent in supporting as many CdS nanoparticles as possible on TiO_2 owing to the lowest polarity.

Removal of the Protective Ligand. The prepared CdS nanoparticles were stabilized in the presence of protective ligands, oleic acid (bp 468 K), and oleyl amine (bp 441 K). We first attempted to remove these protective ligands to improve the accessibility of the CdS surfaces. Figure 3 shows the TG-DTA curves under dry flowing air for 0.072 wt % CdS(3.4)/TiO_2 catalysts with (a) no treatment, (b) heat treatment (HT) at 473 K for 5 h, and (c) alkali treatment (AT) in 0.1 M NaOH solution at 298 K for 1 h. The TG profile for non-treated CdS/TiO_2 (Figure 3a) shows weight loss at 500–700 K, presumably ascribed to the removal of protective ligands such as 9-octadecenylamine and oleic acid and the decomposition of sulfide to oxide. This is consistent with the observed exothermic profile in the corresponding temperature range, as shown in the DTA curve.[33–35] Bulk CdS showed no weight change at 300–900 K (results not shown). Figures 3b and 3c show that HT at 473 K for 5 h and AT drastically reduced the degree of weight loss and exothermicity.

Figure 4 shows UV–vis DRS for (a) TiO_2 (P25) and (b) CdS (Mitsuwa) for reference, and for 0.072 wt % CdS(3.4)/TiO_2 samples with (c) no treatment, (d) HT at 473 K for 5 h, (e) HT at 623 K for 5 h, and (f) AT in 0.1 M NaOH. The absorption band edges of TiO_2 and CdS (Figures 4a and 4b) were 380 and 530 nm corresponding to B.G. of 3.26 and 2.34 eV, respectively. The absorption peak of the as-prepared CdS nanoparticle (3.4 ± 0.4 nm) was 449 nm (B.G. = 2.76 eV), a shorter wavelength by about 90 nm than for bulk CdS (blue shift, ΔB.G. = 0.46 eV) due to the quantum size effect. The observed peaks for 0.072 wt % CdS(3.4)/TiO_2 with (c) no treatment, (d) HT method at 473 K, and (f) AT method remained almost unchanged from that of as-prepared CdS nanoparticles, confirming that the methods successfully immobilized CdS

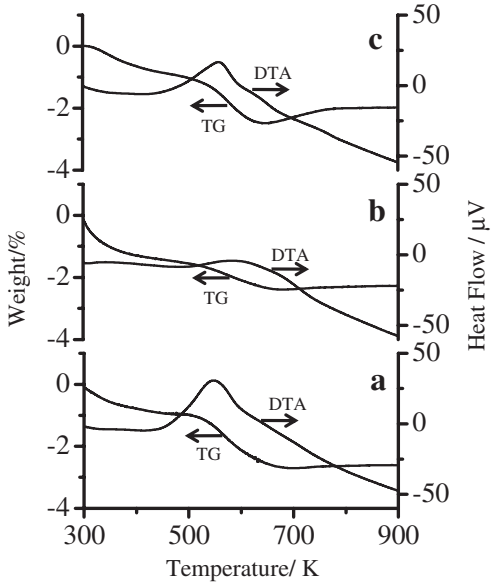

Figure 3. TG-DTA curves under dry flowing air for 0.072 wt % CdS(3.4 ± 0.4)/TiO_2 catalysts with (a) no treatment, (b) heat treatment (HT) at 473 K for 5 h, and (c) alkali treatment (AT) in 0.1 M NaOH solution at 298 K for 1 h.

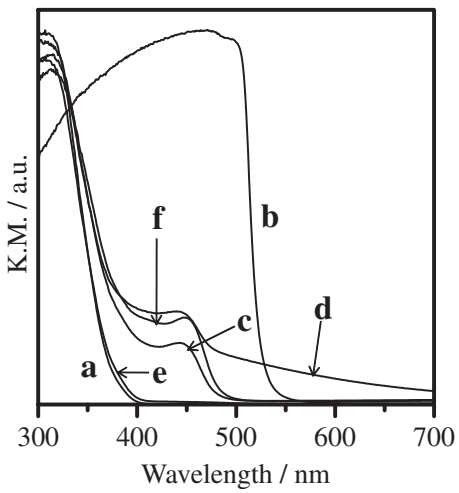

Figure 4. UV–vis DR spectra for (a) TiO_2 (P25), (b) bulk CdS (99.999%, Mitsuwa Chemical), CdS(3.4 ± 0.4)/TiO_2 samples with (c) no treatment, (d) HT at 473 K for 5 h, (e) HT at 623 K for 5 h, and (f) AT in 0.1 M NaOH.

nanoparticles while maintaining the particle size. The absorption at wavelengths beyond the absorption edge of CdS, which was observed for CdS(3.4)/TiO_2 by HT at 473 K, was probably due to reduced Cd species. On the contrary, the absorption by CdS nanoparticles completely vanished, and only adsorption due to TiO_2 was observed after HT at 623 K for 5 h (e). Therefore, HT at 473 K and AT methods were used to remove the protective ligands.

Loading of CdS Nanoparticle. Figure 5 shows UV–vis DRS for 0.072 wt % CdS/TiO_2 prepared with different CdS particle sizes (1.6 ± 0.2 (c), 2.9 ± 0.3 (d), 3.4 ± 0.4 (e), 4.1 ± 0.6 (f), and 12.5 ± 1.6 nm (g)) by HT at 473 K for 5 h as well as (a) TiO_2 (P25) and (b) bulk CdS (Mitsuwa). No

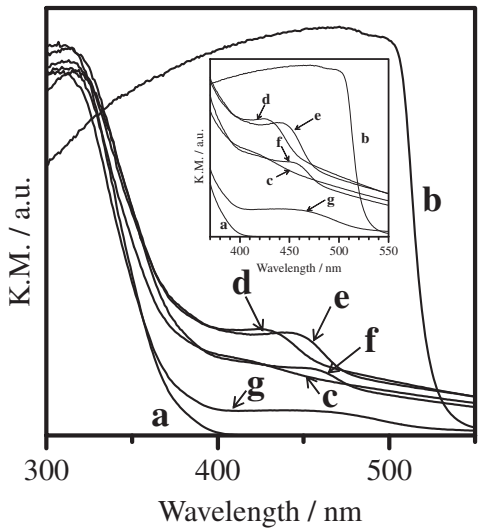

Figure 5. UV–vis DR spectra of (a) TiO_2 (P25), (b) bulk CdS (99.999%, Mitsuwa Chemical), several particle sizes (1.6 ± 0.2 (c), 2.9 ± 0.3 (d), 3.4 ± 0.4 (e), 4.1 ± 0.6 (f), and 12.5 ± 1.6 nm (g)) CdS nanoparticles on TiO_2 by HT method.

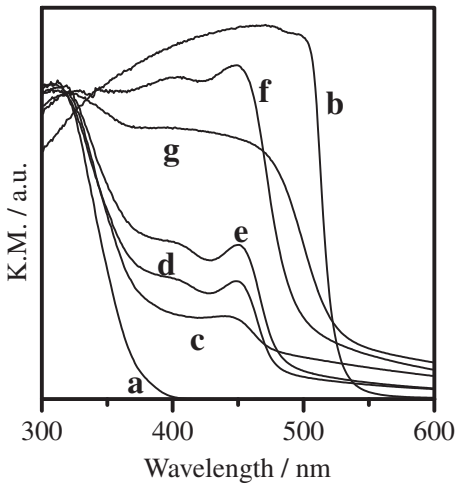

Figure 6. UV–vis DR spectra for (a) TiO_2 (P25), (b) bulk CdS (99.999%, Mitsuwa Chemical), CdS nanoparticles loaded on TiO_2 after HT treatment; The amounts of CdS were (c) 0.072, (d) 0.3, (e) 0.7, (f) 1, and (g) 3 wt %.

absorption due to CdS was observed for CdS(1.6)/TiO_2 (Figure 5c), which originally showed absorption at 370 nm before immobilization. In the case of CdS(1.6)/TiO_2, the absorption above 370 nm was subtly observed whereas the absorption for the unsupported CdS(1.6) did not have absorption in this range. This result indicates that a portion of the CdS(1.6) particles slightly sintered; yet the major portion of CdS(1.6) is still believed to remain constant in size. The CdS(2.9)/TiO_2, CdS(3.4)/TiO_2, and CdS(4.1)/TiO_2 (Figures 5d–5f) showed absorption at 430, 446, and 459 nm, respectively. These absorptions corresponded well to those of the original CdS nanoparticles at 432, 449, and 457 nm for CdS particle sizes of 2.9, 3.4, and 4.1 nm, respectively.[22–24] As seen in Figure 5g, the CdS(12.5)/TiO_2 absorption edge was observed at 540 nm, matching that of the original CdS nanoparticle (12.5 ± 1.6 nm).[22–24] Therefore, it can be concluded that the optical properties and particle size of CdS supported on TiO_2 remained unchanged from the original CdS particles.

We attempted to increase the CdS loading on TiO_2 by starting with CdS with a particle size of 3.4 ± 0.5 nm. Figure 6 shows UV–vis DRS for CdS/TiO_2 (0.072–3 wt % CdS) after HT. The CdS/TiO_2 samples after AT had very similar UV–vis DRS properties (Figure S1, Supporting Information). Absorption was observed at 450 nm in the range 0.072–1 wt % CdS loading (Figure 6). The absorption edge shifted to longer wavelengths with increasing amount of CdS (1–3 wt %). This indicates that the CdS particles aggregated to form larger particles, where the quantum size effect was no longer operative. Assuming the CdS particles were spherical or square in shape, 14.7 or 11.6 wt % of CdS(3.4) could be theoretically loaded to form a CdS monolayer on TiO_2 (P25, 54 $m^2 g^{-1}$), respectively. A surface coverage of 6.8% (sphere) or 8.6% (square) was estimated as the loading at which CdS nanoparticles should begin to aggregate in the current treatments.

Photocatalytic H_2 Evolution Reaction. Table 1 lists the steady-state H_2 evolution rates from 0.1 g of TiO_2 (P25) support only (B.G. = 3.26 eV), 72 μg of CdS nanoparticle colloid without support (B.G. = 2.76 eV), 0.1 g of 0.072 wt % CdS(3.4)/TiO_2 (HT or AT), and 0.1 g of Pt(50) loaded 0.072 wt % CdS(3.4)/TiO_2. No H_2 evolution was detected from TiO_2 support only, due to its obvious lack of visible light response. Although protective ligands should have been removed from CdS particles in Na_2S/Na_2SO_3 solution (pH 13), only negligible H_2 was evolved from CdS nanoparticle colloid (without support), probably because unstable CdS nanoparticles may aggregate easily when they are not immobilized on a support. Supported CdS nanoparticles, on the other hand, had much higher photocatalytic activity (>20 times) than CdS nanoparticles only, although the amounts of CdS in the reaction solution were identical. Moreover, the deposition of Pt on CdS/TiO_2 considerably enhanced the photocatalytic activity (≈5 fold). The photocatalytic activity for CdS/TiO_2 (AT) was about three times higher than that for CdS/TiO_2 (HT). Figure 4 shows that the absorption at the wavelengths beyond the absorption edge ($\lambda > 460$ nm) was observed in the case of CdS/TiO_2 (HT), most likely due to the existence of sulfur defects on the surface. The lack of absorption in this range for CdS/TiO_2 (AT) may indicate the defect sites are much less than those for CdS/TiO_2 (HT), probably accounting for the dif-

Table 1. The Rate of H_2 Evolution from TiO_2 (Support), CdS Nanoparticle, CdS/TiO_2 (No Treatment), CdS/TiO_2 (HT or AT), and Pt/CdS/TiO_2 (HT or AT) in a 200 mL of Solution Containing 0.1 M Na_2S–Na_2SO_3, 0.1 g of Catalyst (CdS: 0.072 wt %, Pt: 50 wt % for CdS) under Irradiation at $\lambda > 420$ nm

Sample	Rate of H_2 evolution/μmol h^{-1}
TiO_2	0
CdS nanoparticle	1
CdS/TiO_2(HT)	23
CdS/TiO_2(AT)	68
Pt/CdS/TiO_2(HT)	104
Pt/CdS/TiO_2(AT)	119

Table 2. The Rate of H_2 Evolution for Several Particle Sizes of CdS (1.6 ± 0.2, 2.9 ± 0.3, 3.4 ± 0.4, 4.1 ± 0.6, and 12.5 ± 1.6 nm) Loaded on TiO_2

Diameter /nm	Band gap /eV	Surface area[a)] /$m^2\,g^{-1}$	H_2 evolution rate[b)] /$\mu mol\,h^{-1}$
1.6 ± 0.2	3.35	778	43(346)
2.9 ± 0.3	2.87	429	60(—)
3.4 ± 0.4	2.76	356	104(227)
4.1 ± 0.6	2.71	304	66(106)
12.5 ± 1.6	2.34	89	2(6)

a) Surface areas are estimated by particle size in assumption to sphere in shape. b) This value in parenthesis is the rate of H_2 evolution under light irradiation ($\lambda > 300$ nm). In the case of CdS(2.9)/TiO_2 was not measured.

ferences in photocatalytic performance. In the case of Pt-deposited samples however, the photocatalytic activity was similar in CdS/TiO_2 (HT) and CdS/TiO_2 (AT), which may indicate that the Pt gives preferential surface sites that do not depend on the CdS defect sites. These results clearly show that immobilization of nanoparticles on a support material is essential to establish their intrinsic activity for photocatalytic reaction.

Unusual properties due to quantum size effects should significantly influence photocatalytic activity, and can be probed by varying CdS particle size. Table 2 shows the H_2 evolution rates of the Pt(50)/0.072 wt% CdS/TiO_2 with starting CdS particle sizes of 1.6 ± 0.2, 2.9 ± 0.3, 3.4 ± 0.4, 4.1 ± 0.6, and 12.5 ± 1.6 nm under visible light and UV light irradiation. Under visible light irradiation, the photocatalytic activity increased as particle size increased up to 3.4 nm, but then began to decrease. Under UV-light irradiation, the photocatalytic activity increased with decreasing particle size. The band gap of CdS nanoparticles measured by UV–vis DRS (Figure 5) and CdS surface area estimated from the particle size assuming a spherical shape are summarized in Table 2. With increasing particle size, the band gaps narrowed due to quantum size effects. On the other hand, the estimated CdS surface area drastically decreases with increasing particle size. It should be noted that 12.5 nm CdS particles exhibited the band gap of bulk CdS material. The photocatalytic activity should be affected by absorptions of visible and UV light by the catalysts, and the ease of oxidation and reduction determined by the positions of the conduction and valence bands of the catalysts. Under UV light irradiation, the H_2 evolution rate decreased with increasing initial CdS particle size, corresponding to a decrease in band gap (i.e., oxidation–reduction ability) and an increase in surface area. Under visible light irradiation, CdS samples with 1.6 nm particles did not have sufficient absorption in the visible light region (absorption: 370 nm), resulting in a comparatively low H_2 evolution rate. By increasing CdS particle size beyond 3.4 nm, the photocatalytic activity decreased because of a depression of the oxidative–reductive power with a narrower band gap. It is notable that nanoparticles exhibiting quantum size effects gave much higher rates than the 12.5 nm CdS sample, which had bulk CdS nature, suggesting that utilization of these nanoparticles had significant benefits for this reaction.

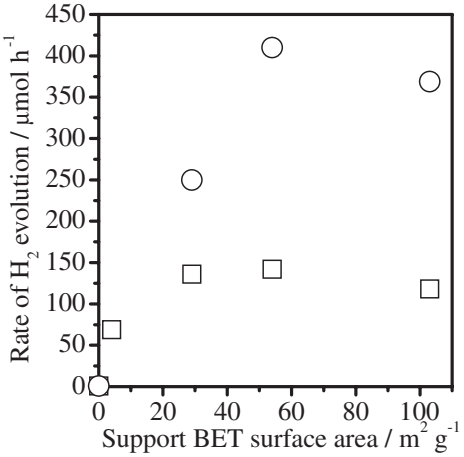

Figure 7. Dependence of the rate of H_2 evolution from Pt (100 wt%)/CdS ((□) 0.072 and (○) 0.3 wt%, particle size = 3.4 nm)/TiO_2 by HT upon the BET surface area; support candidates were rutile ($S_{BET} = 4\,m^2\,g^{-1}$), anatase ($S_{BET} = 29\,m^2\,g^{-1}$), anatase ($S_{BET} = 103\,m^2\,g^{-1}$), and P25 ($S_{BET} = 54\,m^2\,g^{-1}$).

Next, the effects of the TiO_2 support surface area on the photocatalytic activity were investigated. TiO_2 support candidates were rutile ($S_{BET} = 4\,m^2\,g^{-1}$), anatase ($S_{BET} = 29\,m^2\,g^{-1}$), anatase ($S_{BET} = 103\,m^2\,g^{-1}$), and P25 (ca. 70% anatase, 30% rutile, $S_{BET} = 54\,m^2\,g^{-1}$). The H_2 evolution rates for the CdS(3.4)/TiO_2 catalysts are plotted against BET surface area in Figure 7. Without support (plots at $x = 0$ in Figure 7), the photocatalytic activity for CdS nanoparticles was almost negligible, clearly demonstrating the positive effects of CdS nanoparticle dispersion onto the support. Even for the low loading of 0.072 wt%, the H_2 evolution rate was lower for a low-surface-area rutile sample than for other samples with higher surface areas. The comparable rates for the latter samples indicate that nanoparticles were well-dispersed on the support at low CdS loading (0.072 wt%). For 0.3 wt% CdS loaded samples, the photocatalytic activity increased with increasing the surface area of the support by $54\,m^2\,g^{-1}$. It is clear that a higher surface area support can disperse the active CdS species more efficiently, resulting in enhancement of the H_2 evolution rate. 0.3 wt% CdS/TiO_2 samples showed higher activity than 0.072 wt% CdS/TiO_2 samples. Dependence of the rate of H_2 evolution upon the amount of Pt cocatalyst loaded on 0.072 wt% CdS(3.4)/TiO_2 are shown in Figure S2. The Pt(100)-loaded photocatalyst showed high activity.

The H_2 evolution rate is plotted against the amount of CdS(3.4) in HT (a) or AT (b) in Figure 8. The H_2 evolution rates for the catalysts obtained by HT or AT reached maxima when 0.7 or 0.3 wt% of CdS was loaded, respectively. The rate drastically decreased for highly loaded (1 wt%) samples. UV–vis spectra (Figure 6) showed that the absorption shifted to wider wavelength (narrower band gap) compared to samples with lower loading, indicating that particle size increased with increasing amount of CdS, while photocatalytic rates decreased accordingly. These results suggest that the immobilization of CdS nanoparticles exhibiting quantum size effects resulted in high-efficiency H_2 evolution.

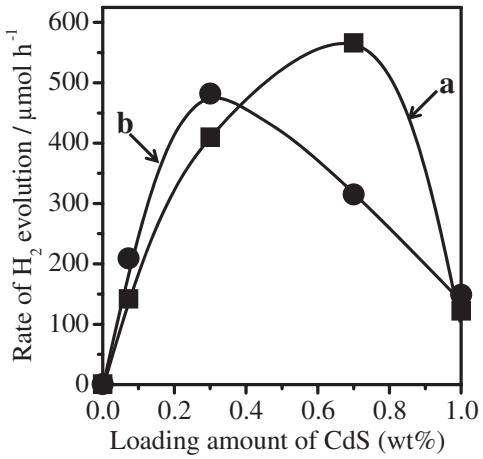

Figure 8. Dependence of the rate of H_2 evolution on the loading amount of CdS in HT (a) or AT (b); Catalyst (0.1 g), Pt (100 wt % for CdS)/CdS (0.072–1 wt %)/TiO_2 (P25); 0.1 M Na_2S–Na_2SO_3 aqueous solution under visible irradiation at $\lambda \geq 420$ nm.

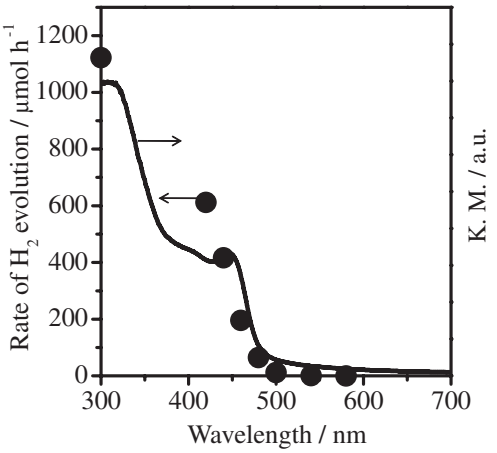

Figure 9. Wavelength dependence of the steady rate of H_2 evolution and UV–vis DRS results for Pt (100 wt % for CdS)/CdS (0.3 wt %)/TiO_2 (P25) with AT followed by HT in a 200 mL of aqueous solution containing 0.1 M Na_2S–Na_2SO_3, 0.1 g of catalyst under visible irradiation at $\lambda \geq 420$ nm.

Finally, we carried out photocatalytic measurements of Pt(100)/0.3 wt % CdS(3.4)/TiO_2 with AT followed by HT at 473 K under visible light irradiation in the presence of Na_2S–Na_2SO_3. This procedure takes advantage of both treatments. The alkali treatment ensures the removal of part of the protective ligands while maintaining the CdS particle size. The remaining protective ligands after the alkali treatment can be further removed by the successive heat treatment with lower exotherm by combustion, thus suppressing creation of sulfur defects than by the direct heat treatment procedure without the alkali treatment.

The rate of H_2 evolution was 616 μmol h^{-1}, the highest value observed in this study, and remained constant for 5 h (Figure S3 in Supporting Information). Figure 9 shows the wavelength dependence of photocatalytic H_2 evolution from aqueous Na_2S–Na_2SO_3 solution over Pt(100)/0.3 wt % CdS(3.4)/TiO_2 catalyst. The H_2 evolution rate decreased with increasing cutoff wavelength, corresponding to excitation at the absorption edge of CdS nanoparticles (3.4 ± 0.4 nm). We confirmed that these photocatalytic H_2 evolution reactions occur by the photogeneration of electrons and holes under visible light irradiation in the presence of Na_2S–Na_2SO_3.

Photoelectrochemical Properties. Figure 10 shows the current–voltage curves for 0.3 wt % CdS(3.4)/TiO_2 sprayed on an FTO electrode compared to bulk CdS (99.999%, Mitsuwa Chemical) in a solution containing Na_2S and Na_2SO_3 as sacrificial electron donors (pH 13) under visible light ($\lambda > 420$ nm). The measurements were conducted by scanning potential from −1.5 to 0 V versus Ag/AgCl. The observed anodic photocurrent is attributed to oxidation of Na_2S and Na_2SO_3, indicating that the CdS(3.4)/TiO_2 functioned as an n-type semiconductor (Figure S4 in Supporting Information). A photocurrent onset for CdS(3.4)/TiO_2 was observed at −1.45 V; a −0.37 V negative shift compared to bulk CdS electrode (−0.108 V). From UV–vis DRS, the band gap of CdS(3.4)/TiO_2 and bulk CdS/TiO_2 were determined to be 2.76 and 2.34 eV, respectively, and the difference in band gap was 0.42 eV, very similar to the difference of onset potential. Thus

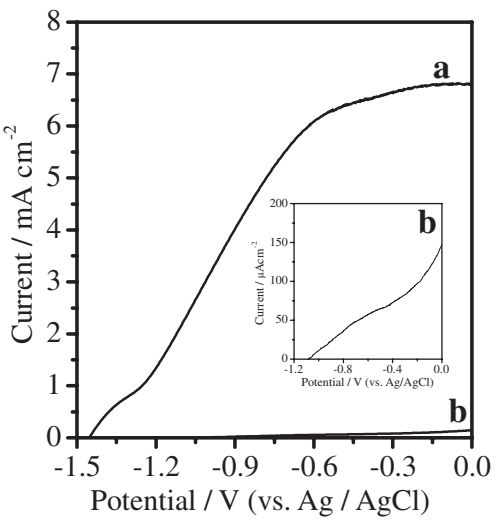

Figure 10. Photocurrent versus voltage of CdS (0.3 wt %)/TiO_2 (P25) after AT followed by HT on FTO in 0.1 M Na_2S–Na_2SO_3 solution at −0.2 V versus Ag/AgCl under visible irradiation at $\lambda \geq 420$ nm.

the difference in band gap mainly originated from the difference in conduction edges, and the positions of the valence bands of CdS(3.4)/TiO_2 and bulk CdS/TiO_2 were very similar, as reported previously.[17] The large difference in photocatalytic activity for H_2 evolution between quantum dot CdS(3.4)/TiO_2 and bulk-like CdS(12.5)/TiO_2 as discussed above (Table 2), can be attributed to the high reduction capability of quantum dot CdS derived from a negatively shifted conduction edge. In addition, a large photocurrent was observed for CdS/TiO_2 (6.8 mA cm^{-2} at −0.2 V versus Ag/AgCl) compared to bulk CdS (0.1 mA cm^{-2} at −0.2 V versus Ag/AgCl) under visible light irradiation with the power density 0.49 W cm^{-2} ($\lambda >$ 420 nm), reflects the high reduction capability of quantum dot CdS. The effect may be attributed to charge separation by TiO_2

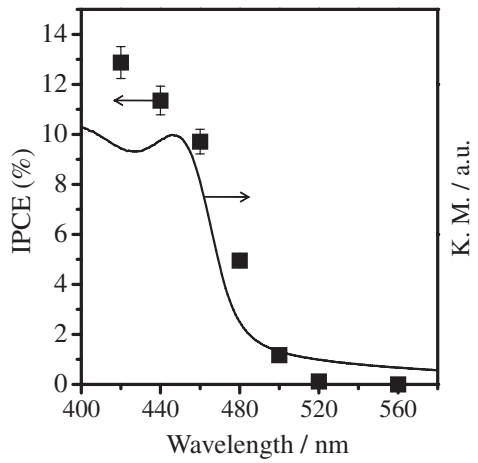

Figure 11. Wavelength dependence of IPCE and UV–vis DRS results for CdS (0.3 wt %)/TiO_2 (P25) with AT followed by HT on FTO in 0.1 M Na_2S–Na_2SO_3 solution at −0.2 V versus Ag/AgCl under visible irradiation at $\lambda \geq 420$ nm.

and the migration without barriers between quantum dot CdS and TiO_2 support when photoexcited electrons transfer to the TiO_2 support.[29,31] There is a possibility that the CdS particles on the grain boundary between TiO_2 particles may cause loss of the photoanodic currents. We cannot rule out that the currents may be improved by a further optimized preparation method of the electrode: for instance, the synthesis of the TiO_2 thin layer prior to CdS introduction should avoid the resistance due to CdS present between the grain boundaries of TiO_2, thus improving photoelectrochemical performance.

Figure 11 shows the dependence of IPCE (−0.2 V versus Ag/AgCl) on the cutoff wavelength of incident light for the 0.3 wt % CdS/TiO_2 electrode. The incident photon-to-photocurrent efficiency, IPCE, is defined by the following eq 2.

$$IPCE(\%) = \frac{hc}{e}\frac{i_{photo}}{\lambda \Phi} \times 100 \quad (2)$$

where i_{photo}, λ, and Φ are photocurrent density (A m^{-2}), wavelength (m), and light flux (W m^{-2}), and c, h, and e are the speed of light (2.998×10^8 m s^{-1}), Plank's constant (6.626×10^{-34} W s), and the elementary electric charge (1.602×10^{-19} A s). A monochromatic light source (Asahi Spectra MAX-301) was used with a bandpath filter (half bandwidth: ±10 nm) in the wavelength region of 420 to 560 nm. The DRS results for the 0.3 wt % CdS(3.4)/TiO_2 powder are also shown. Photocurrent was observed at up to 500 nm, and the variation in photocurrent with respect to wavelength was in good agreement with the DRS results. The observed photocurrent can thus be attributed to a photoelectrochemical oxidation reaction via the band gap transition of CdS. The IPCE at 420 nm for CdS/TiO_2 at −0.2 V versus Ag/AgCl was thus derived to be 12.9%.

Conclusion

CdS nanoparticles dispersed on TiO_2 to maintain particle size were successfully prepared by heat treatment and alkali treatment to effectively remove protective ligands. The photocatalytic measurements suggest that CdS/TiO_2 catalyzed the reduction of H^+ to H_2 under visible light irradiation in the presence of a sacrificial electron donor (Na_2S–Na_2SO_3). Quantum size effects in CdS particles on TiO_2 were observed from 1.6 to 4.1 nm (1.6 ± 0.2, 2.9 ± 0.3, 3.4 ± 0.4, and 4.1 ± 0.6 nm), and the photocatalytic activity was maximum at 3.4 ± 0.4 nm, about fifty times higher than 12.5 ± 1.6 nm CdS with similar properties to bulk CdS. To further investigate the preparation method, the loading amount of CdS or Pt and several supports with different surface areas were examined. The photocatalytic activity was 616 μmol h^{-1} at Pt (100 wt % for CdS)/CdS (0.3 wt %)/TiO_2 (P25, $S_{BET} = 54$ m^2 g^{-1}) after alkali treatment followed by heat treatment. For CdS/TiO_2 on an FTO electrode, photoanodic current (6.8 mA cm^{-2}) was measured in the presence of 0.1 M Na_2S–Na_2SO_3 under visible light irradiation with the power density 0.49 W cm^{-2} ($\lambda > 420$ nm). It was shown that CdS functions as a high activity n-type semiconductor. The high efficiency was attributed not only to quantum size effects, but also to charge separation due to the difference between the bottoms of the conduction bands of CdS and TiO_2. There is still a large margin for photocatalytic activity improvement by optimizing type and surface area of the support with supplementary deposition of CdS. The knowledge acquired in this study can be applied for general usage of organic-ligand-protected nanoparticle materials.

This work was supported in part by Global COE Program (Chemistry Innovation through Cooperation of Science and Engineering), MEXT, Japan.

Supporting Information

UV–vis DR spectra for CdS/TiO_2 after AT (Figure S-1). Time course of H_2 evolution of several aliquots of Pt loaded on CdS/TiO_2 (Figure S-2). Time course of H_2 evolution for Pt(100)/0.3 wt % CdS(3.4)/TiO_2 with AT followed by HT (Figure S-3). (a) Current–time at −0.2 V vs. Ag/AgCl and (b) current–potential curves for 0.3 wt % CdS(3.4)/TiO_2 on FTO electrode (Figure S-4). This material is available free of charge on the Web at: http://www.csj.jp/journals/bcsj/.

References

1 A. Fujishima, K. Honda, *Nature* **1972**, *238*, 37.
2 K. Domen, A. Kudo, T. Onishi, *J. Catal.* **1986**, *102*, 92.
3 A. Kudo, H. Kato, *Chem. Phys. Lett.* **2000**, *331*, 373.
4 J. F. Reber, K. Meier, *J. Phys. Chem.* **1984**, *88*, 5903.
5 A. Kudo, A. Nagane, I. Tsuji, H. Kato, *Chem. Lett.* **2002**, 882.
6 I. Tsuji, H. Kato, H. Kobayashi, A. Kudo, *J. Am. Chem. Soc.* **2004**, *126*, 13406.
7 R. J. Williams, *J. Chem. Phys.* **1960**, *32*, 1505.
8 H. Gerischer, *J. Electroanal. Chem.* **1975**, *58*, 263.
9 J. R. Wilson, S.-M. Park, *J. Electrochem. Soc.* **1982**, *129*, 149.
10 J. R. Darwent, *J. Chem. Soc., Faraday Trans. 2* **1981**, *77*, 1703.
11 J. R. Harbour, R. Wolkow, M. L. Hair, *J. Phys. Chem.* **1981**, *85*, 4026.
12 T. Inoue, T. Watanabe, A. Fujishima, K. Honda, K. Kohayakawa, *J. Electrochem. Soc.* **1977**, *124*, 719.
13 H. Minoura, M. Tsuiki, *Electrochim. Acta* **1978**, *23*, 1377.

14 K. R. Gopidas, M. Bohorquez, P. V. Kamat, *J. Phys. Chem.* **1990**, *94*, 6435.
15 S. Hotchandani, P. V. Kamat, *J. Phys. Chem.* **1992**, *96*, 6834.
16 A. Eychmüller, A. Hässelbarth, H. J. Weller, *J. Lumin.* **1992**, *53*, 113.
17 L. E. Brus, *J. Chem. Phys.* **1984**, *80*, 4403.
18 Y. Nosaka, *J. Phys. Chem.* **1991**, *95*, 5054.
19 Y. Wang, *Acc. Chem. Res.* **1991**, *24*, 133.
20 A. Henglein, *Chem. Rev.* **1989**, *89*, 1861.
21 Al. L. Efros, A. L. Efros, *Sov. Phys. Semicond.* **1982**, *16*, 772.
22 T. Teranishi, M. Saruyama, M. Kanehara, *Chem. Lett.* **2009**, *38*, 194.
23 J. Joo, H. B. Na, T. Yu, J. H. Yu, Y. W. Kim, F. Wu, J. Z. Zhang, T. Hyeon, *J. Am. Chem. Soc.* **2003**, *125*, 11100.
24 M. Kanehara, H. Arakawa, R. Hironaga, T. Teranishi, *Trans. Mater. Res. Soc. Jpn.* **2006**, *31*, 437.
25 S. G. Hickey, D. J. Riley, E. J. Tull, *J. Phys. Chem. B* **2000**, *104*, 7623.
26 T. Hirai, Y. Bando, I. Komasawa, *J. Phys. Chem. B* **2002**, *106*, 8967.
27 J. C. Yu, L. Wu, J. Lin, P. Li, Q. Li, *Chem. Commun.* **2003**, 1552.
28 J. C. Tristão, F. Magalhães, P. Corio, M. T. C. Sansiviero, *J. Photochem. Photobiol., A* **2006**, *181*, 152.
29 S. Chen, M. Paulose, C. Ruan, G. K. Mor, O. K. Varghese, D. Kouzoudis, C. A. Grimes, *J. Photochem. Photobiol., A* **2006**, *177*, 177.
30 J. S. Jang, W. Li, S. H. Oh, J. S. Lee, *Chem. Phys. Lett.* **2006**, *425*, 278.
31 H. Park, W. Choi, M. R. Hoffmann, *J. Mater. Chem.* **2008**, *18*, 2379.
32 C.-F. Chi, Y.-L. Lee, H.-S. Weng, *Nanotechnology* **2008**, *19*, 125704.
33 P. J. Sebastian, M. E. Calixto, *Thin Solid Films* **2000**, *360*, 128.
34 F. El-Tantawy, K. M. Abdel-Kader, F. Kaneko, Y. K. Sung, *Eur. Polym. J.* **2004**, *40*, 415.
35 L. Yang, Q. Shen, J. Zhou, K. Jiang, *Mater. Lett.* **2005**, *59*, 2889.